

# CDVAE: Co-embedding Deep Variational Auto Encoder for Conditional Variational Generation

Jiajun Lu, Aditya Deshpande, David Forsyth  
University of Illinois at Urbana Champaign  
{jlu23, ardeshp2, daf}@illinois.edu

## Abstract

Problems such as predicting an optical flow field ( $Y$ ) for an image ( $X$ ) are ambiguous: many very distinct solutions are good. Representing this ambiguity requires building a conditional model  $P(Y|X)$  of the prediction, conditioned on the image. It is hard because training data usually does not contain many different flow fields for the same image. As a result, we need different images to share data to produce good models. We demonstrate an improved method for building conditional models, the Co-Embedding Deep Variational Auto Encoder. Our CDVAE exploits multiple encoding and decoding layers for both  $X$  and  $Y$ . These are tied during training to produce a model of the joint distribution  $P(X, Y)$ , which provides the necessary smoothing. Our tying procedure is designed to yield a conditional model easy at test time. We demonstrate our model on three example tasks using real data: image saturation adjustment, image relighting, and motion prediction. We describe quantitative evaluation metrics to evaluate ambiguous generation results. Our results quantitatively and qualitatively advance the state of the art.

## 1. Introduction

Many vision problems have ambiguous solutions. There are many motion fields consistent with an image [17, 22, 23]. Similarly, there are many shading fields consistent with the layout of an image (this paper); many good ways to colorize an image [25]; many good ways to adjust the saturation of an image (this paper); many possible long term futures for an image frame [26]; and so on. For each of these problems, one must produce a spatial field  $Y$  for an image  $X$ ; but  $Y$  is not uniquely determined by  $X$ . Worse,  $Y$  has complex spatial structure (for example, motion at a pixel is typically similar to motion at the next pixel, except over boundaries). It is natural to build a generative model of  $Y$ , conditioned on  $X$ , and draw samples from that model. The very high dimension and complex spatial covariances of  $Y$

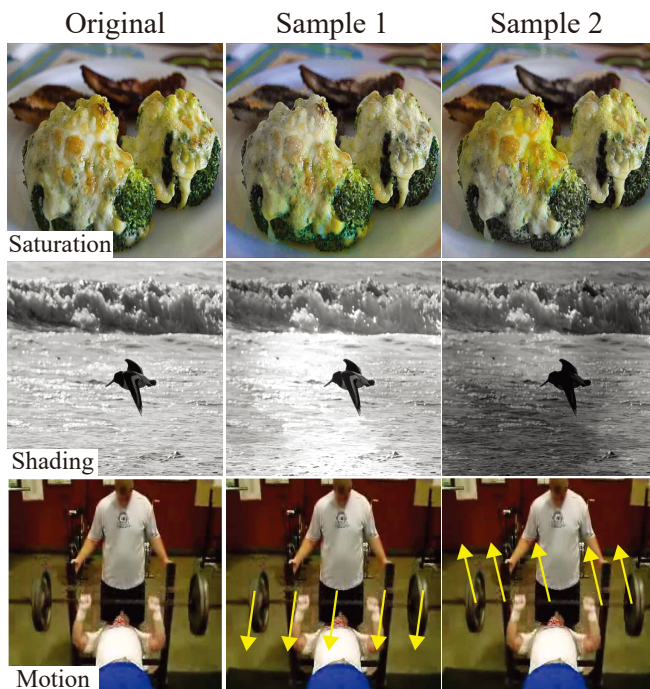


Figure 1. We describe a method to learn a multimodal conditional distribution  $P(Y|X)$  for “scattered” data, where in examples one never sees two distinct  $y$  values for a given  $x$  value. Our method allows us to produce new saturation fields for images, reshade images, and predict motion fields for images.

are managed by building a latent variable model. Recent work has modified a strong generative model for images that uses latent variables, the variational auto-encoder (VAE) of [7], to produce a conditional VAE (CVAE [17, 22, 23]).

However, building a conditional model is difficult. An important difficulty in most practical vision problems is that the training dataset we can access is “scattered”: training data consists of pairs of  $(y_i, x_i)$ , but we never see multiple different values of  $y_i$  for one particular  $x_i$ . Worse, in interesting cases  $P(Y|X)$  is not even unimodal. Just training a high capacity predictor using a log likelihood criterion (or variational approximation) will distort the space of  $X$  to

push distant  $x_i$  with similar  $y_i$  together and similar  $x_i$  with different  $y_i$  apart. The result is a poor model with good log-likelihood on training data. Such a model will have difficulty producing diverse solutions (experiments confirm the significance of this effect, section 6).

To build a plausible conditional model, we must oblige examples with similar  $x_i$  to “share”  $y$  values, however different the  $y$  values are. Such smoothing needs to be controlled. This is easier to do in a joint model than in a conditional model. However, building a joint model may lead to a conditional model that is hard to sample. An attraction of CDVAE is that one does not need Markov chain Monte Carlo methods to draw samples. In this paper, we describe an approach that allows us to train a joint model (and so smooth in a sensible way), but easily pass to a conditional model at generation time.

We obtain our model by training two deep variational auto-encoders using a novel tying procedure and a novel regularization procedure. Tying is chosen to ensure that: (a) the generative model can produce appropriate  $Y$ ; (b)  $Y$  is conditioned on a useful representation of  $X$ ; and (c) at run time, the tie can be coerced into a conditional model. We regularize our model by initializing the VAE codes to have good metric properties. This ensures that very different examples are embedded far apart; the method can move them closer if doing so is essential, but only in that case. Our approach conveniently extends to multiple layers of latent variables, and we use the Deep VAE of [14] for our problems. We call our model a CDVAE (Co-Embedding Deep Variational Auto Encoder).

We demonstrate our model on three problems. One is established: we must predict a motion field consistent with a static image [17, 22, 23]. The other two are novel: in reshading, we decompose the image into shading and albedo, then produce a new shading field consistent with the albedo field; in resaturation, we produce a new saturation field and apply it to the image. In each case, the resulting image should look “natural” – like a real image, but differently illuminated (reshading) or with differently saturated objects (resaturation). In all cases, our model strongly outperforms natural baselines which themselves outperform CVAEs.

### Contributions:

- We describe a novel method to build conditional models for extremely demanding datasets. Our method builds a joint distribution with controllable smoothing, in a way that yields a conditional model that is easy to sample.
- We show how to regularize our model so that the latent representation is not distorted, and this helps us improve results.
- Our method is compared to a variety of natural base-

lines, and produces predictions that (a) have high variance and (b) have high accuracy. Our method clearly outperforms existing models.

## 2. Related Work

Generating a spatial field with complex spatial structure from an image is an established problem. Important application examples, where the prediction is naturally ambiguous, include colorization [3, 9, 25], style transfer [4], temporal transformations prediction [26], predicting motion fields [17, 22, 23], and predicting future frames [21]. This is usually treated as a regression problem; current state of the methods use deep networks to learn features. However, predicting the expected value of a conditional distribution works poorly, because the expected value of a multimodal distribution may have low probability. While one might temper the distribution (eg [25]), the ideal is to obtain multiple different solutions.

One strategy is to draw samples from a generative model. Generative models of images present problems of dimension; these can be addressed with latent variable models, leading to the variational autoencoder (VAE) of [7]. As the topic attracts jargon, we review the standard VAE briefly here. This approach learns an encoder  $E$  that maps data  $x$  into a continuous latent variable  $z = E(x)$  (the codes), and a decoder  $D$  that maps  $z$  to an image  $\hat{x} = D(z)$ . Learning ensures that (a)  $x$  and  $D(E(x))$  are close; (b) if  $\xi$  is close to  $z$ , then  $D(\xi)$  is close to  $D(z)$ ; and (c)  $z$  is distributed like a standard normal random variable. Images can then be generated by sampling a standard normal distribution to get  $\xi$ , and forming  $D(\xi)$ . This is a latent variable model, modelling  $P(x)$  as  $P(x) = \int_z P(x|z)P(z)dz$  where  $P(x|z)$  is represented by the decoder, and  $P(z|x)$  is represented by the encoder. Learning is by maximizing a bound on log-likelihood. Writing  $Q = P(z|x)$ , we have

$$\text{VAE}(\theta) = \sum_{data} [\mathbb{E}_Q \log P(x|z) - \mathbb{D}(Q||P(z))] \quad (1)$$

where  $\theta$  are the parameters of encoder and decoder networks.

Current generative models are reliable in simple domains (handwritten digits [7, 16]; faces [7, 8, 14]; and CIFAR images [5]) but less so for general images. Improvements are available using multiple layers of latent variables (a DVAE) [14]. Models can be trained adversarially [13]. However, these deep models are still hard to train. The ladder VAE imposes both top-down and bottom up variational distributions for more efficient training [18].

The generative model needs to be conditioned on an image, and needs to be multimodal. Tang et al. give a conditional model [19], but the conditioning variables are binary. A conditional variational autoencoder (CVAE) [17] conditions the decoder model on a representation produced by a

network applied to  $x$ . This approach has been demonstrated on motion prediction problems [22, 26].

We use the mixture density network (MDN) in our models [2]. An MDN predicts the parameters of a mixture of gaussians from real-valued input features. MDNs have been successfully applied to articulatory-acoustic inversion mapping [15, 20] and speech synthesis [24].

### 3. Method

Our CDVAE utilizes multiple layers of gaussian latent variables, like the deep variational auto encoder (DVAE) [14] (refer to Figure 2). This hierarchical architecture captures complex structure in the data, and has a good record in practice. We write  $\text{DVAE}(\theta)$  for the variational cost of a DVAE, which is derived in the same way of a VAE. We use an inference method [18] that co-relates the latent variables in encoder side and decoder side to speed up the training process and make the network able to utilize more of the multiple layer latent variables. Refer to support materials for details. Generally, we distinguish between the generated image layer (motion; saturation; shading) and the conditioning image layer (intensity; albedo) by subscripts (so  $x_c$  is a conditioning image layer,  $x_g$  is a generated image layer, etc.).

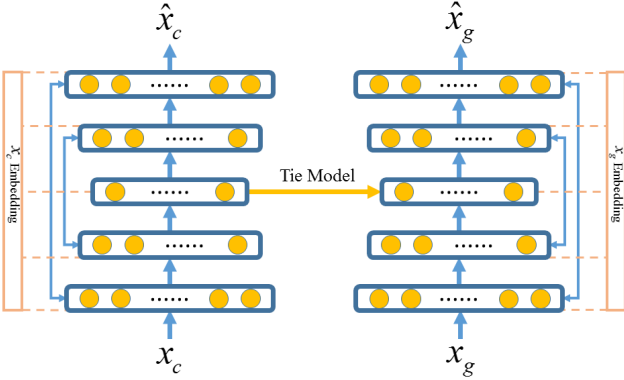


Figure 2. The architecture of our CDVAE network. **Left** our DVAE for the conditioning layer  $x_c$ ; **right** our DVAE for the generated layer  $x_g$ . Each DVAE has three layers of latent gaussian variables, and these latent layers are connected by two fully connected layers and leaky rectifiers. For each DVAE, the corresponding latent gaussian layers are related to facilitate learning, as in [18]. Our CDVAE model uses a joint model to tie the two DVAEs to perform joint training, and the joint model turns into a conditional model at test time.

The architecture of our CDVAE model is in Figure 2. We wish to build a joint model  $P(x_c, x_g)$  such that a conditional model  $P(x_c|x_g)$  is easy to get. In CDVAE, we use two multi-layer variational auto encoders (DVAE),

one for  $x_c$  and one for  $x_g$ . We use latent variables for each of them and model the joint probability  $P(x_c, x_g)$  as  $\int_z P(x_c|z_c)P(x_g|z_g)P(z_g, z_c)dz_gdz_c$ .

#### 3.1. Tied Models

Now we consider the joint probability  $P(x_c, x_g)$ . Assume it is possible to encode  $x_c$  without seeing  $x_g$ , then the variational distribution  $Q = P(z_c|x_c)P(z_g|x_g)$  applies. If  $P(z_g, z_c) = P(z_g)P(z_c)$ , we can build two separate VAE's, because the integral decomposes (supplementary material). If we have

$$\log P(z_g, z_c) = -\frac{z_c^T z_c}{2} - \frac{z_g^T z_g}{2} - F_{\text{tie}}(z_c, z_g)$$

Write  $\text{DVAE}(\theta_c)$  for the DVAE loss for the  $x_c$  model (same for  $x_g$ ), and following the derivation of VAE yields a training loss

$$\mathcal{L}_{\text{CDVAE}} = \text{DVAE}(\theta_c) + \text{DVAE}(\theta_g) + \text{Tie}(\theta_c, \theta_g) \quad (2)$$

where

$$\text{Tie}(\theta_c, \theta_g) = \sum_{\text{data}} E_Q F_{\text{tie}}(z_c, z_g).$$

This equals that we train two DVAEs, but tying their latent variables with an appropriately chosen cost. Below, we describe two tying methods that each leads to simple conditional models.

**The Gaussian Tie** In this model, we tie 80% components of the codes. Write  $z_c^t$  and  $z_g^t$  for the tied components, which can be chosen without loss of generality. We choose

$$\log P(z_c, z_g) = -\frac{z_c^T z_c}{2} - \frac{z_g^T z_g}{2} - \frac{\|z_g^t - z_c^t\|^2}{2\sigma_t^2}. \quad (3)$$

Applying the standard variational criteria with the  $\log P(z_c, z_g)$ , we can transform our loss function  $\mathcal{L}$  into

$$\mathcal{L}_{\text{CDVAE,gauss}} = \text{DVAE}(\theta_c) + \text{DVAE}(\theta_g) + \sum_{i \in \text{data}} \frac{\|z_{g,i}^t(\theta_g) - z_{c,i}^t(\theta_c)\|^2}{2\sigma_t^2}. \quad (4)$$

The resulting conditional model is

$$P(x_g|x_c) = \int_z P(x_g|z_g)P(z_g|z_c)P(z_c|x_c)dz_gdz_c. \quad (5)$$

where  $P(x_g|z_g)$  is the decoder and  $P(z_c|x_c)$  is the encoder. Since the joint model linking  $z_c$  and  $z_g$  is normal,  $P(z_g|z_c)$  is normal distribution, too. This means the resulting conditional model is easy to sample. We draw from the gaussian distribution  $z_g^t = \mathcal{N}(z_c^t, \sigma_t^2)$  for tied codes and  $z_g^{ut} = \mathcal{N}(0, 1)$  for untied codes.

**The MDN Tie** Our second approach to model the joint distribution is mixture density network [2]. It models the

probability distribution as a mixture of Gaussians, allowing a multimodal conditional distribution. We tie all the components of the  $z_c$  and  $z_g$  with an MDN. For each input code  $z_c$ , our MDN estimates the parameters of a  $K$  component mixture density distribution with mixture coefficients  $\pi_i$ , means  $\mu_i$  and fixed diagonal covariance  $\sigma_i^2$ . The tying process described above is general and the same derivation applies to MDN tie; we add an MDN tie loss

$$\mathcal{L}_{mdn} = -E_Q \left[ \log \sum_{k=1}^K \pi_k(z_c) \mathcal{N}(z_g | \mu_k(z_c), \sigma_k^2(z_c)) \right] \quad (6)$$

to obtain

$$\mathcal{L}_{CDVAE,mdn} = \text{DVAE}(\theta_c) + \text{DVAE}(\theta_g) + \mathcal{L}_{mdn}(\theta_c, \theta_g). \quad (7)$$

Since the joint model linking  $z_c$  and  $z_g$  is a mixture of normal distributions,  $P(z_g|z_c)$  is a mixture of normal distributions, too. This means the resulting conditional model is also easy to sample.

## 4. Practical Considerations

There are two important implementation details. First, we use embedding guidance to regularize the code space. Second, we post process generated images for viewing at high resolution.

### 4.1. Embedding Guidance

Codes in a VAE appears to be underdetermined, especially for large and various datasets. This is because the encoder and decoder have high capacity, which creates optimization problems. The VAE is easily trapped in local minima, and has difficulty in generating a coherent code embedding space. For our conditional models, we should like codes for “similar” inputs to be nearby, and codes for “very different” inputs to be far apart. This discourages the method from grouping together very different inputs with similar outputs to get good losses. We also observe that the code space for the VAE models are flexible and it’s easy to guide the codes in embedding while still keep them coherent.

We construct the guidance vector by building a feature vector  $f$  and perform dimension reduction which preserves the locality of the data points. Our feature vector  $f$  contains three parts: semantic information, image layout and raw pixels, refer to Figure 3. The semantic part is object label percentage in the image (sum to 1). The layout part is object bounding box spatial layout. We map the object bounding boxes into  $5 \times 5$  coarse grids to achieve compactness, and use the coverage percentage of each category on each grid to represent the feature vector. The third part is resized  $32 \times 32$  image pixels. Finally, we reweight the semantic part and layout part higher, and concatenate these features to get the feature vector  $x$ . For MS-COCO dataset,

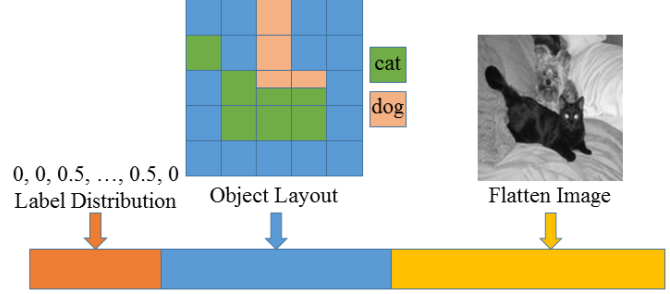


Figure 3. Our feature vector is constructed by three parts. First part is label distribution, which describes the object label percentages in the image, such as 0.5 cat and 0.5 dog. Second part is object layout, which includes information of spatial layout percentages. The last part is resized image pixels, which provides low level image information.

we use features  $f_c = [f_{label}, f_{bbox}, f_{img}]$  for conditional layer  $x_c$ , and features  $f_g = [f_{img}]$  for generation layer  $x_g$ . For UCF101 dataset, we do not include term  $f_{bbox}$ .

We use Niyogi et al’s LPP [12] to build an embedding which preserves metric relations between data points. We construct our adjacency graph as  $W_{ij} = e^{-\frac{\|f_i - f_j\|^2}{t}}$ , and follow the paper’s procedures to get low dimension embedding  $p$ . We charge the VAE for using codes that are far away from the codes predicted by the embedding, with cost

$$\text{Embedding}(z) = \|z - p\|^2 \quad (8)$$

The embedding guidance cost is large at beginning to initialize the code space, and then cools down to make the VAE costs dominate. By doing so, we discourage major distortions of the metric, without preventing them. We see our approach as similar to batch normalization [6], which discourages (but does not prevent) large values between layers. We can use the embedding guidance to customize the code space to the applications. This embedding guidance brings an regularizer term  $\text{Embedding}(z)$  to the loss function, so our loss function  $\mathcal{L}$  becomes

$$\mathcal{L} = \mathcal{L}_{CDVAE} + \lambda \text{Embedding}(z) \quad (9)$$

where weights  $\lambda$  starts with a big number and gradually reduces to near zero during the training process. Our testing process does not have embedding guidance and embedding cost.

### 4.2. Post Processing

All measurements of errors are made on the outputs of generative models. However, current deep generative models only handle small images, and generate results without high spatial frequencies. For visual results only, we perform post processing to generate results at high resolution



of  $512 \times 512$  and with more details. We aggressively up-sample the generated fields with method [11], which preserves edges during upsampling. In particular the method represents a high resolution field by a weight and an orientation value at each sample point; these parameters control a basis function placed at each sample, and the field at any test point is a sum of the values of the basis functions at that point. The sum of basis functions includes only those basis functions in the same image segment. Write  $\text{Interp}(\mathbf{w}, \theta; \mathcal{S}(I))$  for the high resolution field produced by interpolating a weight vector  $\mathbf{w}$  and a vector of orientations  $\theta$ , assuming a segment mask  $\mathcal{S}(I)$  obtained from the high resolution grey level image. Write  $Y^{(d)}$  for a low resolution field produced by the decoder, and  $\downarrow G_\sigma$  for a process that smoothes and downsamples. We solve

$$\downarrow G_\sigma * (\text{Interp}(\mathbf{w}, \theta; \mathcal{S}(I))) = Y^{(d)}$$

for  $\mathbf{w}, \theta$ , regularizing with the magnitude of  $\mathbf{w}$ . This produces a high resolution field that (a) is compatible with the high resolution edges of the grey level image (unlike the learned upsampling in common use) and (b) produces the decoder sample when smoothed.

For relighting and saturation adjustment tasks, we polish images for display by using detail maps to recover fine scale details. The detail map is calculated by that the original layer  $I_o$  subtracts the output produced by the CDVAE with a ground truth codes  $z_o$ . This captures the high frequency details lost during the neural network process. We get our result  $\hat{I}_g$  as

$$\hat{I}_g = \text{CDVAE}(z_g) + (I_o - \text{CDVAE}(z_o)) \quad (10)$$

## 5. Applications

We apply our methods to three different ambiguous tasks, each of which admits both quantitative and qualitative evaluations.

**Photo Relighting:** In this application, we predict new shading fields for images which are consistent with a relit version of the scene. We decompose the image into albedo (the conditioning layer  $x_c$ ), and shading (the generated layer  $x_g$ ). In real images, shading is quite strongly conditioned by albedo because the albedo image contains semantic information such as the scene categories, objects layout and potential light sources. A scene can be lighted in multiple ways, so relighting is a multimodal problem. We use the MS-COCO dataset for relighting.

**Image Resaturation:** In this application, we predict new saturation fields for color images, modifying color saturation for some or all objects in the image. We transfer the color image into hsv color space, and use the value channel as our conditioning layer and the saturation channel as our generated layer. This allows us to generate new versions of

an image where some colors in some locations have different saturations (such as the grilled cheese on the broccoli in Figure 1). Our model learns saturation distributions across multiple images to obtain natural choices of resaturation for a particular image. We use the MS-COCO dataset for this application.

**Motion Prediction:** This is an established application: predicting a motion field from a single image. The color image is the conditioning layer and the motion field is the generated layer. We follow [22] in using the UCF101 dataset to allow comparison to earlier methods.

## 6. Results

To evaluate the effectiveness of our method, we compare with recent strong methods and with variants of our method in applications of photo relighting, image resaturation and motion prediction. Quantitative results are reported without post-processing. Images shown for qualitative evaluation of resaturation and reshading are postprocessed, as in section 4.2.

### 6.1. Datasets

**MS-COCO:** We use MS-COCO dataset for our tasks of photo relighting and image resaturation. It is a wild and complex dataset that is challenging for VAE methods. We use train2014 (80K images) for model training, and use val2014 (40K images) for testing. For photo relighting, intrinsic method [1] is used to perform decomposition, and for image resaturation, we transform the image from RGB space to HSV space to perform operations.

**UCF101:** We use UCF101 dataset for motion prediction. Both our training data and testing data come from UCF101, and we use first annotation train/test split. Our motions are calculated with optical flow [10] for frames of one second interval. For each video, we sample eight images equally, and get a training dataset of 80K images and a testing dataset of 30K images.

We resize all the images to  $32 \times 32$  dimensions, and all operations before post processing are performed on this size of images. After our CDVAE model generates samples, we use post processing to aggressively upsample the image [11] to the resolution of  $512 \times 512$ .

### 6.2. Baseline Methods

**Nearest neighbor search:** We perform nearest neighbor search in  $x_c$  space, and return the corresponding  $x_g$  as results. Gaussian smoothing is applied to returned  $x_g$  to remove uncontrollable high frequency signal. Since our training data does not have one to multiple correspondences, nearest neighbor search is a natural strong baseline.

**Conditional variational autoencoder:** Our implementation of the CVAE [22] uses 5 convolutional layers for both

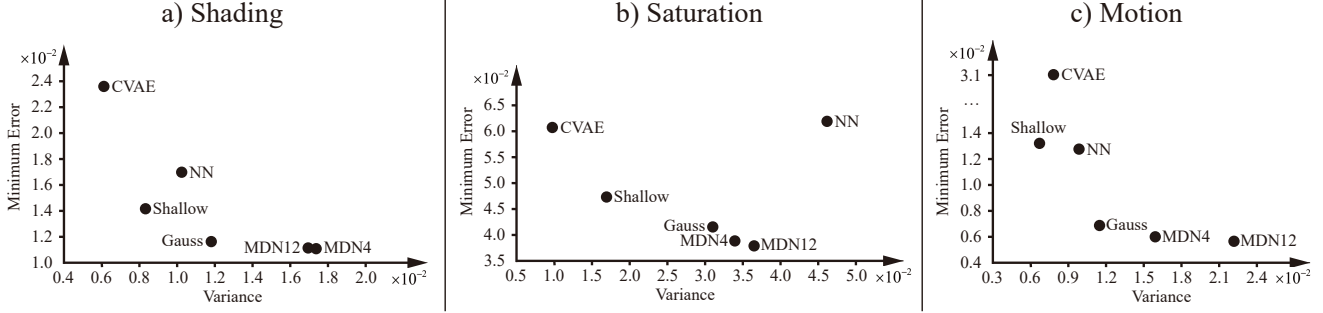


Figure 4. Comparison to baselines on three tasks: a) is for photo relighting, b) is for image resaturation, and c) is for motion prediction. Vertical axis is distance of closest sample to ground truth (smaller is better), and horizontal axis is variance of predicted samples (bigger is better). Both are calculated with 100 samples. In all tasks, CVAE fails to generate near ground truth samples and has low variance for generated results, suggesting the method is poor at producing diverse samples. The nearest neighbor creates variance but cannot predict samples close to ground truth. For our methods and variations, the performance increases as the model goes deeper and has stronger tying model. Tables with detailed numbers are in the support materials.

image tower and encoder tower. We train with pixel wise L2 loss and our model does not produce direct negative loglikelihood.

**Shallow CDVAE:** Our CDVAE model uses multiple layers of latent gaussian variables, and we compare with a “shallow model” that uses one layer of latent variables. Doing so demonstrates the effectiveness of deep latent variables. Our shallow model (one layer of latent variables) uses a gaussian tie.

### 6.3. Quantitative Evaluation

We perform qualitative and quantitative comparisons on our results of all three tasks. For quantitative evaluation, we report negative loglikelihood, best error to ground truth and variance of sample points.

**Negative log likelihood:** Our implementation of CVAE does not have explicit negative log likelihood, and some previous works use Parzen window method to estimate it. However, such estimation is highly inaccurate because of the high dimension, so we do not report our negative loglikelihood for CVAE, and only use the result from motion prediction paper [22]. Numbers are reported in Table 1. For motion prediction, our method and variations outperform CVAE method. Generally, as our model goes deeper and use stronger conditional model, the negative log likelihood becomes smaller.

**Best error to ground truth:** We follow the motion prediction work [22] to use best error to ground truth as an evaluation metric. We draw 100 samples for each conditional layer and calculate the minimum per pixel error to ground truth fields. A better model will produce smaller values, because it should produce some samples close to ground truth.

**Variance:** The main point of the paper is to produce diverse samples. We evaluate diversity by evaluating a vari-

$-\log p(x_c, x_g)$	CVAE	Shallow	Gauss	MDN4	MDN12
shading	n/a	2373	1932	1854	1821
saturation	n/a	1593	1284	1105	1078
motion	11082	7425	6489	6449	6517

Table 1. Negative loglikelihood directly reported by models (smaller number is better). Our implementation of CVAE does not directly report negative loglikelihood, so we have this number only for motion prediction from paper [22]. Our CDVAE produces smaller negative loglikelihood as the model goes deeper, and MDN “tie” is generally better than gaussian “tie”.

ance term. We obtain the values for 16 equal spaced grid points across 100 samples, and compute the variance at each grid point across samples, and average the variances. While these variances are incomparable across problems, they can be compared for different methods for a given problem. In particular, more diverse solutions should produce higher variances.

We include comparisons on best error to ground truth and variance for three tasks in Figure 4. In all tasks, our CDVAE model creates results that has smallest best error to ground truth and largest variance. Our CDVAE model produces better results as the model goes deeper for latent gaussian variable layers, and uses stronger conditional models.

### 6.4. Qualitative Evaluation

Our method produces not only state of the art quantitative results, but also strong qualitative results. Our CDVAE model automatically learns the semantic information and layout of the images and embeds this information into the code space. Samples from our jointly trained conditional model smooth information across “similar” images, allowing us to produce aligned, semantically sensible and reasonable samples. Our qualitative comparisons with other



Figure 5. Qualitative comparisons for tasks of photo relighting, photo resaturation and motion prediction. The first column is input image for conditional variational generation. For tasks of relighting and saturation adjustment, our detail map is applied. If the model keeps outputting a same result with any input, the generated image will be the original image. Nearest neighbor creates worst visual results in relighting and saturation adjustment tasks, because there is no enough data compared to the high dimension feature space, and the method has little awareness of content and spatial layout. CVAE generates less various results, and has difficulty at generating novel good solutions. Both our CDVAE with Gaussian “tie” and CDVAE with MDN “tie” generates multimodal good results. In the task of motion prediction, both our CDVAEs creates more reasonable predictions.

methods for three tasks is shown in Figure 5. In all tasks, our method creates state of the art visual results.

**Photo Relighting:** We show our photo relighting results with CDVAE and four mixture components MDN “tie” in Figure 6. For each input image, we draw four samples from the distribution. The photo relighting results show that our CDVAE model learns the light source distributions as well as important objects. Our model creates light fields coming from reasonable light sources and the lighting looks reasonable, especially on important objects.

**Image Resaturation:** Our image saturation adjustment results with CDVAE and twelve mixture components MDN “tie” are shown in Figure 7. For each input image, we draw four samples from the distribution. The saturation adjustment results show that our model learns multimodal saturation distributions effectively. Our automatic saturation adjustment creates appealing photos and brings artistic stylization effects.

**Motion Prediction:** Our motion prediction results with CDVAE and a gaussian tie are shown in Figure 8. Given an input video frame from UCF101 dataset, we draw four samples from the distribution, and recover the motion fields. Because videos in the UCF101 dataset usually have an unstable camera view, there are lots of small motions in the whole frame. We use arrows to represent big motion fields. All the areas near the arrows share a similar motion field. The results show that our model generates multimodal and reasonable motions by understanding the image frame content and matching to similar images in the learned local manifold.

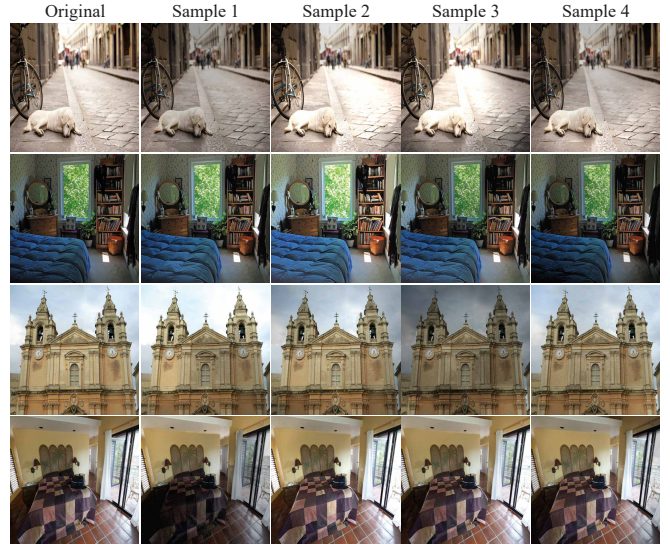


Figure 6. Input images in the first column are relighted with four samples from our CDVAE model with four mixture components MDN “tie”. Our CDVAE model automatically learns the potential places of light sources, scene layouts and important objects without supervision. This information is important for arranging light sources in the right spot, shading the scene in the right way and highlighting important objects. Our conditional distribution model captured the relationship between this information and shading fields, and by sampling the distribution, we creates multiple distinct reasonable solutions. In the examples, light comes mainly from windows and sky, and objects are correctly relighted.



## 7. Discussion

Our CDVAE generates state of the art results qualitatively and quantitatively, however, there is still some limitations. Some of them are due to neural network properties and are hard to fix, and some of them could be fixed in potential future works. First, variational auto-encoders and variants **oversmooth** their outputs. Our deep latent gaussian distribution architecture can capture more complex structures, but the output still misses details compared to ground truth. Second, our model – like all current generative models – is applied to **low resolution** images, meaning that much structural and semantic information important to obtaining good results is lost. Last, our model has **no spatial hierarchy**. Coarse to fine multiscale hierarchy model on both generative side and conditional side would likely to enable us generate results with more details.

## 8. Conclusion

We have described an important approach that simplifies building conditional models by building a joint model, which yields a conditional model that can be easily sampled. This allows us to train scattered data using a joint model, so we can easily control the smoothing of data. We have shown how to apply this approach to state of the art image layer generative models. We also proposed an approach to regularize code space to make it coherent for conditional generative models. With all these novel techniques, our CDVAE method brings significant improvements in the diversity and accuracy of the model’s output, and creates qualitatively and quantitatively state of the art results.

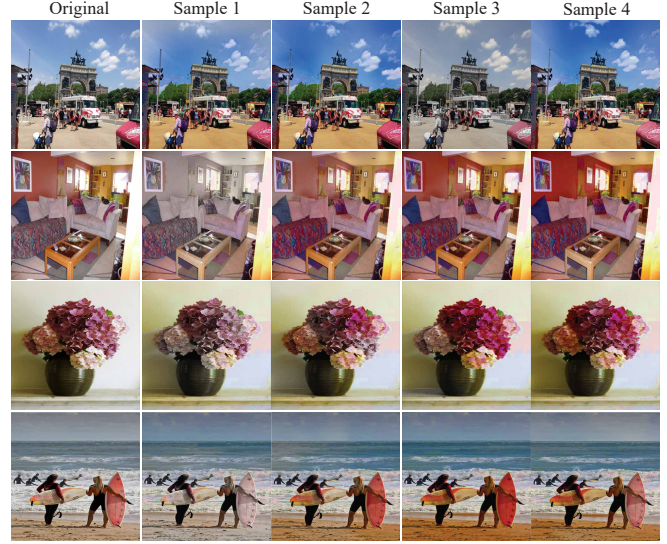


Figure 7. Each input image in the first column takes four samples from our CDVAE model with twelve mixture components MDN “tie”. Our CDVAE model automatically generates multimodal saturation adjustments by sampling a conditional distribution which is joint learned from MS-COCO dataset and captures dependencies of layouts and saturation choices. In the example, the generated saturation layers respect objects and has reasonable spatial layout and magnitude, making the results appealing.

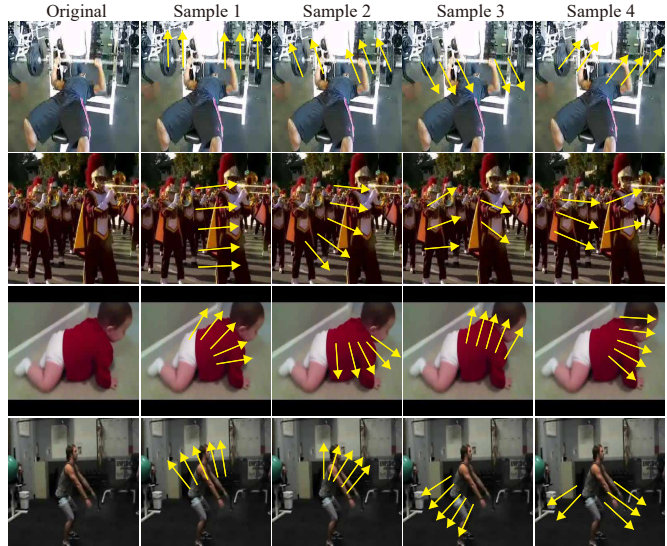


Figure 8. Motion prediction is ambiguous, and for each input image in the first column, we predict four motions (based on clustered samples) with our gaussian “tie” CDVAE model. Our CDVAE model automatically figures out the scene content and performs a multimodal prediction based on our joint trained conditional gaussian “tie” model. In the examples, big motions are visualized and image fields near the arrows share the same predicted motion of the arrow. As we can see, the predicted motions are all reasonable and distinct solutions.



## 9. Appendix

### 9.1. DVAE

The difference between DVAE [14] and VAE [7] is more layers of gaussian latent variables. DVAE for  $x_c$  (same for  $x_g$ ) consists of  $L$  layers of latent variables. To generate a sample from the model, we begin at the top-most layer ( $L$ ) by drawing from a Gaussian distribution to get  $z_{c,L}$ .

$$P(z_{c,L}) = \mathcal{N}(z_{c,L}|0, I) \quad (11)$$

The mean and variance for the Gaussian distributions at any lower layer is formed by a non-linear transformation of the sample from above layer.

$$\mu_{c,i} = f_{\mu_{c,i}}(z_{c,i+1}) \quad (12)$$

$$\sigma_{c,i}^2 = f_{\sigma_{c,i}^2}(z_{c,i+1}) \quad (13)$$

where  $f$  represents multi-layer perceptrons. We descend through the hierarchy by one hot vector sample process.

$$z_{c,i} = \mu_{c,i} + \xi_i \sigma_{c,i} \quad (14)$$

where  $\xi_i$  are mutually independent Gaussian variables.  $x_c$  is generated by sampling from the Gaussian distribution at the lowest layer.

$$P(x_c|z_{c,1}) = \mathcal{N}(x_c|\mu_{c,0}, \sigma_{c,0}^2) \quad (15)$$

The joint probability distribution  $P(x_c, z_c)$  of this model is formulated as

$$\begin{aligned} P(x_c, z_c) &= P(x_c|z_{c,1})P(z_c) \\ &= P(x_c|z_{c,1})P(z_{c,L}) \prod_{i=1}^{L-1} P(z_{c,i}|z_{c,i+1}) \end{aligned} \quad (16)$$

where  $P(z_{c,i}|z_{c,i+1}) = \mathcal{N}(z_{c,i}|\mu_{c,i}, \sigma_{c,i}^2)$ . In other places, DVAE and VAE models are same.

#### 9.1.1 Inference

DVAE with several layers of dependent stochastic variables are difficult to train which limits the improvements obtained using these highly expressive models. LVAE [18] recursively corrects the generative distribution by a data dependent approximate likelihood in a process resembling the recent Ladder Network. It utilizes a deeper more distributed hierarchy of latent variables and captures more complex structures. We follow this work and for  $x_c$ , write  $\mu_{c,p,i}$  and  $\sigma_{c,p,i}^2$  for the mean and variance on the  $i$ 's level of generative side, write  $\mu_{c,q,i}$  and  $\sigma_{c,q,i}^2$  for the mean and variance on the  $i$ 's level of inference side.

This changes the notation in the previous part on the generative side.

$$P_p(z_c) = P_p(z_{c,L}) \prod_{i=1}^{L-1} P_p(z_{c,i}|z_{c,i+1}) \quad (17)$$

$$P_p(z_{c,L}) = \mathcal{N}(z_{c,L}|0, I) \quad (18)$$

$$P_p(z_{c,i}|z_{c,i+1}) = \mathcal{N}(z_{c,i}|\mu_{c,p,i}, \sigma_{c,p,i}^2) \quad (19)$$

$$P_p(x_c|z_{c,1}) = \mathcal{N}(x_c|\mu_{c,p,0}, \sigma_{c,p,0}^2) \quad (20)$$

On the inference side, the notation also changes.

$$P_q(z_c|x_c) = P_q(z_{c,1}|x_c) \prod_{i=2}^L P_q(z_{c,i}|z_{c,i-1}) \quad (21)$$

$$P_q(z_{c,1}|x_c) = \mathcal{N}(z_{c,1}|\mu_{c,q,1}, \sigma_{c,q,1}^2) \quad (22)$$

$$P_q(z_{c,i}|z_{c,i-1}) = \mathcal{N}(z_{c,i}|\mu_{c,q,i}, \sigma_{c,q,i}^2) \quad (23)$$

During inference, first a deterministic upward pass computes the approximate distribution  $\hat{\mu}_{c,q,i}$  and  $\hat{\sigma}_{c,q,i}^2$ . This is followed by a stochastic downward pass recursively computing both the approximate posterior and generative distributions.

$$P_q(z_c|x_c) = P_q(z_{c,L}|x_c) \prod_{i=1}^{L-1} P_q(z_{c,i}|z_{c,i+1}) \quad (24)$$

$$\sigma_{c,q,i} = \frac{1}{\hat{\sigma}_{c,q,i}^{-2} + \sigma_{c,p,i}^{-2}} \quad (25)$$

$$\mu_{c,q,i} = \frac{\hat{\mu}_{c,q,i} \hat{\sigma}_{c,q,i}^{-2} + \mu_{c,p,i} \sigma_{c,p,i}^{-2}}{\hat{\sigma}_{c,q,i}^{-2} + \sigma_{c,p,i}^{-2}} \quad (26)$$

$$P_q(z_{c,i}|\cdot) = \mathcal{N}(z_{c,i}|\mu_{c,q,i}, \sigma_{c,q,i}^2) \quad (27)$$

where  $\mu_{c,q,L} = \hat{\mu}_{c,q,L}$  and  $\sigma_{c,q,L}^2 = \hat{\sigma}_{c,q,L}^2$ .

### 9.2. Tied Models

First, we will prove that independent joint probability leads to two separate DVAEs. Then, we will prove the derivations for tied model.

### 9.2.1 Seperate DVAEs

From Section 3 in the paper, we have joint probability  $P(x_c, x_g)$  in CDVAE model as

$$P(x_c, x_g) = \int_z P(x_c|z_c)P(x_g|z_g)P(z_g, z_c)dz_gdz_c \quad (28)$$

If  $z_c$  and  $z_g$  are independent, and  $P(z_g, z_c) = P(z_g)P(z_c)$ , replace in Equation 28, we have

$$\begin{aligned} P(x_c, x_g) &= \int_z P(x_c|z_c)P(x_g|z_g)P(z_g)P(z_c)dz_gdz_c \\ &= \int_z (P(x_c|z_c)P(z_c))dz_c(P(x_g|z_g)P(z_g))dz_g \\ &= \int_{z_c} P(x_c|z_c)P(z_c)dz_c + \int_{z_g} P(x_g|z_g)P(z_g)dz_g \\ &= P(x_c) + P(x_g) \end{aligned} \quad (29)$$

where  $P(x_c)$  is DVAE model for  $x_c$  and  $P(x_g)$  is DVAE model for  $x_g$ .

### 9.2.2 Tied Model Derivation

From Section 2 in the paper, we have objective function for VAE as

$$\text{VAE}(\theta) = \sum_{data} [\mathbb{E}_Q \log P(x|z) - \mathbb{D}(Q||P(z))] \quad (30)$$

where  $Q = P(z|x)$ . Applying the same derivations for our joint model, we have objective function for our CDVAE as

$$\text{CDVAE}(\theta_c, \theta_g) = \sum_{data} [\mathbb{E}_Q \log P(x_c, x_g|z_c, z_g) - \mathbb{D}(Q||P(z_c, z_g))] \quad (31)$$

where  $Q = P(z_c, z_g|x_c, x_g)$ . Assume it is possible to encode  $x_c$  without seeing  $x_g$ , then the variational distribution  $Q = P(z_c|x_c)P(z_g|x_g)$  applies. We also assume it is possible to decode  $x_c$  without seeing  $x_g$ , then we have  $P(x_c, x_g|z_c, z_g) = P(x_c|z_c)P(x_g|z_g)$ . Applying these formulas to Equation 31, we have

$$\begin{aligned} \mathbb{E}_Q \log P(x_c, x_g|z_c, z_g) &= \mathbb{E}_Q \log(P(x_c|z_c)P(x_g|z_g)) \\ &= \mathbb{E}_{Q_1} \log P(x_c|z_c) \\ &\quad + \mathbb{E}_{Q_2} \log P(x_g|z_g) \end{aligned} \quad (32)$$

where  $Q_1 = P(z_c|x_c)$  and  $Q_2 = P(z_g|x_g)$ . We have  $\log P(z_c, z_g) = \log P(z_c) + \log P(z_g) + F_{\text{tie}}(z_c, z_g)$ , then

we have the following equations for the second part.

$$\begin{aligned} \mathbb{D}(Q||P(z_c, z_g)) &= \mathbb{D}(P(z_c|x_c)P(z_g|x_g)||P(z_c, z_g)) \\ &= \mathbb{E}_Q(\log(P(z_c|x_c)P(z_g|x_g)) - \log P(z_c, z_g)) \\ &= \mathbb{E}_{Q_1}(\log P(z_c|x_c)) + \mathbb{E}_{Q_2}(\log P(z_g|x_g)) \\ &\quad - \mathbb{E}_{Q_1}(\log P(z_c)) - \mathbb{E}_{Q_2}(\log P(z_g)) \\ &\quad - \mathbb{E}_Q(F_{\text{tie}}(z_c, z_g)) \\ &= \mathbb{D}(Q_1||P(z_c)) + \mathbb{D}(Q_2||P(z_g)) \\ &\quad - \mathbb{E}_Q(F_{\text{tie}}(z_c, z_g)) \end{aligned} \quad (33)$$

In our case, we have  $\log P(z_c) = -\frac{z_c^T z_c}{2}$  and  $\log P(z_g) = -\frac{z_g^T z_g}{2}$  because of gaussian distribution. Our CDVAE objective function turns into

$$\text{CDVAE}(\theta_c, \theta_g) = \text{DVAE}(\theta_c) + \text{DVAE}(\theta_g) + \sum_{data} \mathbb{E}_Q(F_{\text{tie}}(z_c, z_g)) \quad (34)$$

### 9.3. Quantitative Results

The detailed quantitative evaluation results corresponding to Figure 4 in the paper could be found here: **photo relighting** results refer to Table 2, **image resaturation** results refer to Table 3 and **motion prediction** results refer to Table 4. The first parts of three tables are best errors to ground truth, with different sample numbers. As the sample number increases, the error drops fast at beginning, and then becomes stable. Our CDVAEs are consistently better than other methods. As the latent layers go deeper and tie model becomes stronger, our CDVAE tends to perform better. The second parts of three tables are average variances at 16 fixed points across 100 samples. Since the variance almost does not change with the sample number, we use the number comes from 100 samples.

### 9.4. Qualitative Results

We include more qualitative results corresponding to Figure 6, Figure 7, and Figure 8 in the paper. For **photo relighting**, results are samples from our CDVAE model with four mixture components MDN "tie", refer to Figure 9, Figure 10, Figure 11. For **image resaturation**, results are samples from our CDVAE model with twelve mixture components MDN "tie", refer to Figure 12, Figure 13, Figure 14. For **motion prediction**, results are samples from our CDVAE model with Gaussian "tie", refer to Figure 15, Figure 16.

## References

- [1] S. Bell, K. Bala, and N. Snavely. Intrinsic images in the wild. *ACM Trans. Graph.*, 33(4):159:1–159:12, July 2014.
- [2] C. M. Bishop. Mixture density networks. 1994.
- [3] A. Deshpande, J. Rock, and D. Forsyth. Learning large-scale automatic image colorization. In *Proceedings of the IEEE International Conference on Computer Vision*, pages 567–575, 2015.
- [4] L. A. Gatys, A. S. Ecker, and M. Bethge. A neural algorithm of artistic style. *arXiv preprint arXiv:1508.06576*, 2015.
- [5] K. Gregor, I. Danihelka, A. Graves, D. J. Rezende, and D. Wierstra. Draw: A recurrent neural network for image generation. *arXiv preprint arXiv:1502.04623*, 2015.
- [6] S. Ioffe and C. Szegedy. Batch normalization: Accelerating deep network training by reducing internal covariate shift. *arXiv preprint arXiv:1502.03167*, 2015.
- [7] D. P. Kingma and M. Welling. Auto-encoding variational bayes. *arXiv preprint arXiv:1312.6114*, 2013.
- [8] T. D. Kulkarni, W. F. Whitney, P. Kohli, and J. Tenenbaum. Deep convolutional inverse graphics network. In *Advances in Neural Information Processing Systems*, pages 2539–2547, 2015.
- [9] G. Larsson, M. Maire, and G. Shakhnarovich. Learning representations for automatic colorization. *arXiv preprint arXiv:1603.06668*, 2016.
- [10] C. Liu. *Beyond pixels: exploring new representations and applications for motion analysis*. PhD thesis, Citeseer, 2009.
- [11] J. Lu and D. Forsyth. Sparse depth super resolution. In *2015 IEEE Conference on Computer Vision and Pattern Recognition (CVPR)*, pages 2245–2253. IEEE, 2015.
- [12] X. Niyogi. Locality preserving projections. 2004.
- [13] A. Radford, L. Metz, and S. Chintala. Unsupervised representation learning with deep convolutional generative adversarial networks. *arXiv preprint arXiv:1511.06434*, 2015.
- [14] D. J. Rezende, S. Mohamed, and D. Wierstra. Stochastic backpropagation and approximate inference in deep generative models. *arXiv preprint arXiv:1401.4082*, 2014.
- [15] K. Richmond. Trajectory mixture density networks with multiple mixtures for acoustic-articulatory inversion. In *International Conference on Nonlinear Speech Processing*, pages 263–272. Springer, 2007.
- [16] T. Salimans et al. Markov chain monte carlo and variational inference: Bridging the gap.
- [17] K. Sohn, H. Lee, and X. Yan. Learning structured output representation using deep conditional generative models. In *Advances in Neural Information Processing Systems*, pages 3483–3491, 2015.
- [18] C. K. Sønderby, T. Raiko, L. Maaløe, S. K. Sønderby, and O. Winther. Ladder variational autoencoders. *arXiv preprint arXiv:1602.02282*, 2016.
- [19] Y. Tang and R. R. Salakhutdinov. Learning stochastic feed-forward neural networks. In *Advances in Neural Information Processing Systems*, pages 530–538, 2013.
- [20] B. Uria, I. Murray, S. Renals, and K. Richmond. Deep architectures for articulatory inversion.
- [21] C. Vondrick, H. Pirsaviash, and A. Torralba. Anticipating the future by watching unlabeled video. *arXiv preprint arXiv:1504.08023*, 2015.
- [22] J. Walker, C. Doersch, A. Gupta, and M. Hebert. An uncertain future: Forecasting from static images using variational autoencoders. In *European Conference on Computer Vision*, pages 835–851. Springer, 2016.
- [23] T. Xue, J. Wu, K. L. Bouman, and W. T. Freeman. Visual dynamics: Probabilistic future frame synthesis via cross convolutional networks. *arXiv preprint arXiv:1607.02586*, 2016.
- [24] H. Zen and A. Senior. Deep mixture density networks for acoustic modeling in statistical parametric speech synthesis. In *2014 IEEE International Conference on Acoustics, Speech and Signal Processing (ICASSP)*, pages 3844–3848. IEEE, 2014.
- [25] R. Zhang, P. Isola, and A. A. Efros. Colorful image colorization. *arXiv preprint arXiv:1603.08511*, 2016.
- [26] Y. Zhou and T. L. Berg. Learning temporal transformations from time-lapse videos. In *European Conference on Computer Vision*, pages 262–277. Springer, 2016.

	Best Error to Ground Truth					Variance
	Sample# 3	Sample# 10	Sample# 30	Sample# 60	Sample# 100	Sample#
NN	3.04	2.30	1.93	1.76	1.66	1.04
CVAE	3.44	2.93	2.61	2.48	2.39	0.61
Shallow	2.51	1.94	1.63	1.49	1.40	0.83
Gauss	2.15	1.63	1.35	1.24	1.16	1.19
MDN4	2.44	1.66	1.33	1.20	1.11	1.77
MDN12	2.49	1.69	1.33	1.20	1.12	1.74

Table 2. Photo relighting results. First part is best error to ground truth with different sample numbers; second part is variance, which is stable with different sample numbers. (all results need  $\times 10^{-2}$ )

	Best Error to Ground Truth					Variance
	Sample# 3	Sample# 10	Sample# 30	Sample# 60	Sample# 100	Sample#
NN	10.12	8.40	7.09	6.52	6.20	4.58
CVAE	8.02	7.14	6.54	6.23	6.04	0.96
Shallow	7.48	6.11	5.33	4.97	4.73	1.64
Gauss	7.39	6.02	4.96	4.45	4.13	3.10
MDN4	6.62	5.11	4.37	4.05	3.86	3.48
MDN12	6.40	5.04	4.33	4.02	3.82	3.55

Table 3. Image resaturation results. First part is best error to ground truth with different sample numbers; second part is variance, which is stable with different sample numbers. (all results need  $\times 10^{-2}$ )

	Best Error to Ground Truth					Variance
	Sample# 3	Sample# 10	Sample# 30	Sample# 60	Sample# 100	Sample#
NN	2.39	1.75	1.45	1.31	1.23	0.95
CVAE	5.33	4.31	3.69	3.38	3.18	0.81
Shallow	2.50	1.89	1.57	1.42	1.32	0.67
Gauss	1.54	1.05	0.81	0.72	0.67	1.19
MDN4	1.36	0.89	0.71	0.63	0.60	1.54
MDN12	1.61	0.92	0.69	0.62	0.58	2.28

Table 4. Motion prediction results. First part is best error to ground truth with different sample numbers; second part is variance, which is stable with different sample numbers. (all results need  $\times 10^{-2}$ )



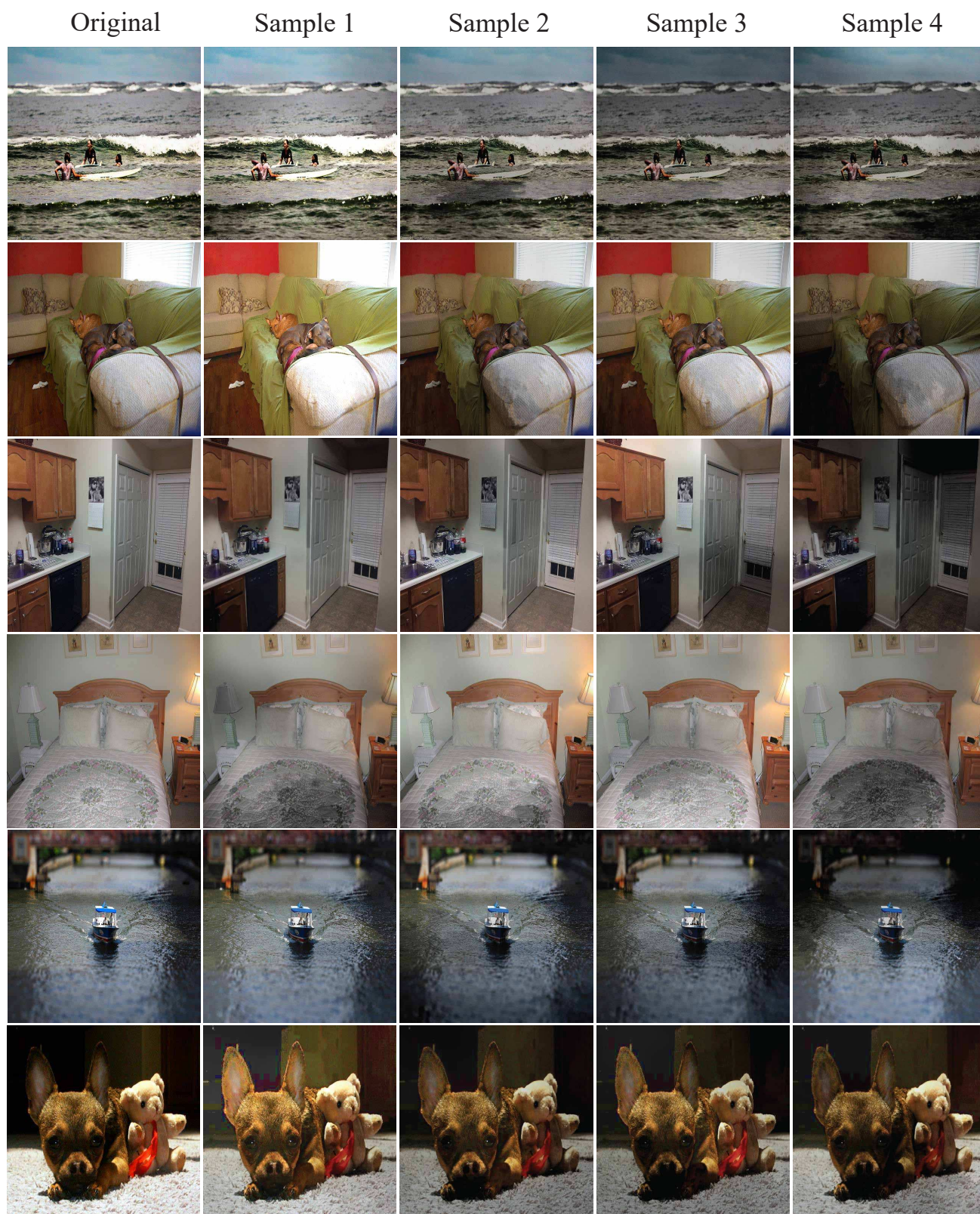


Figure 9. Photo relighting results part 1.



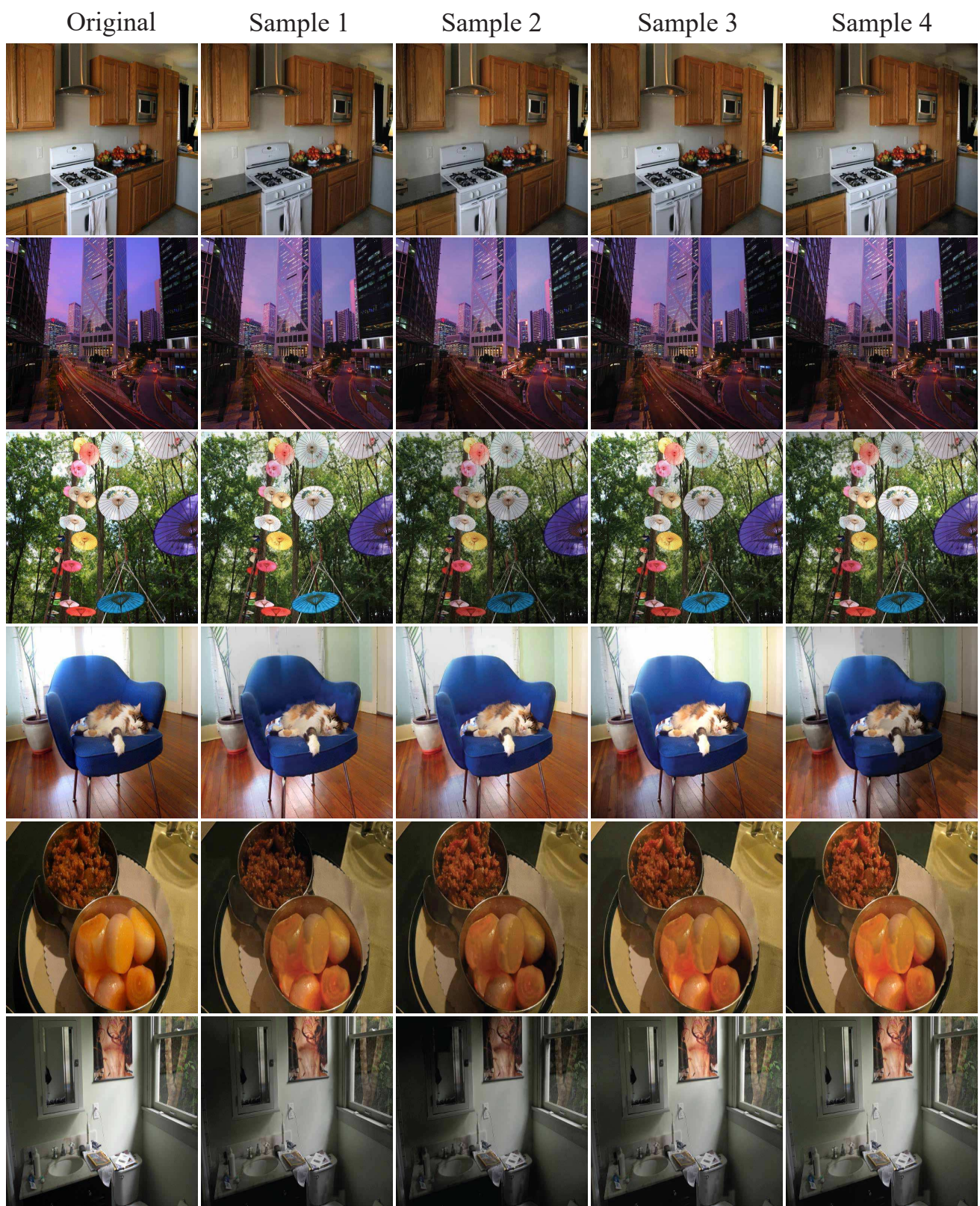


Figure 10. Photo relighting results part 2.



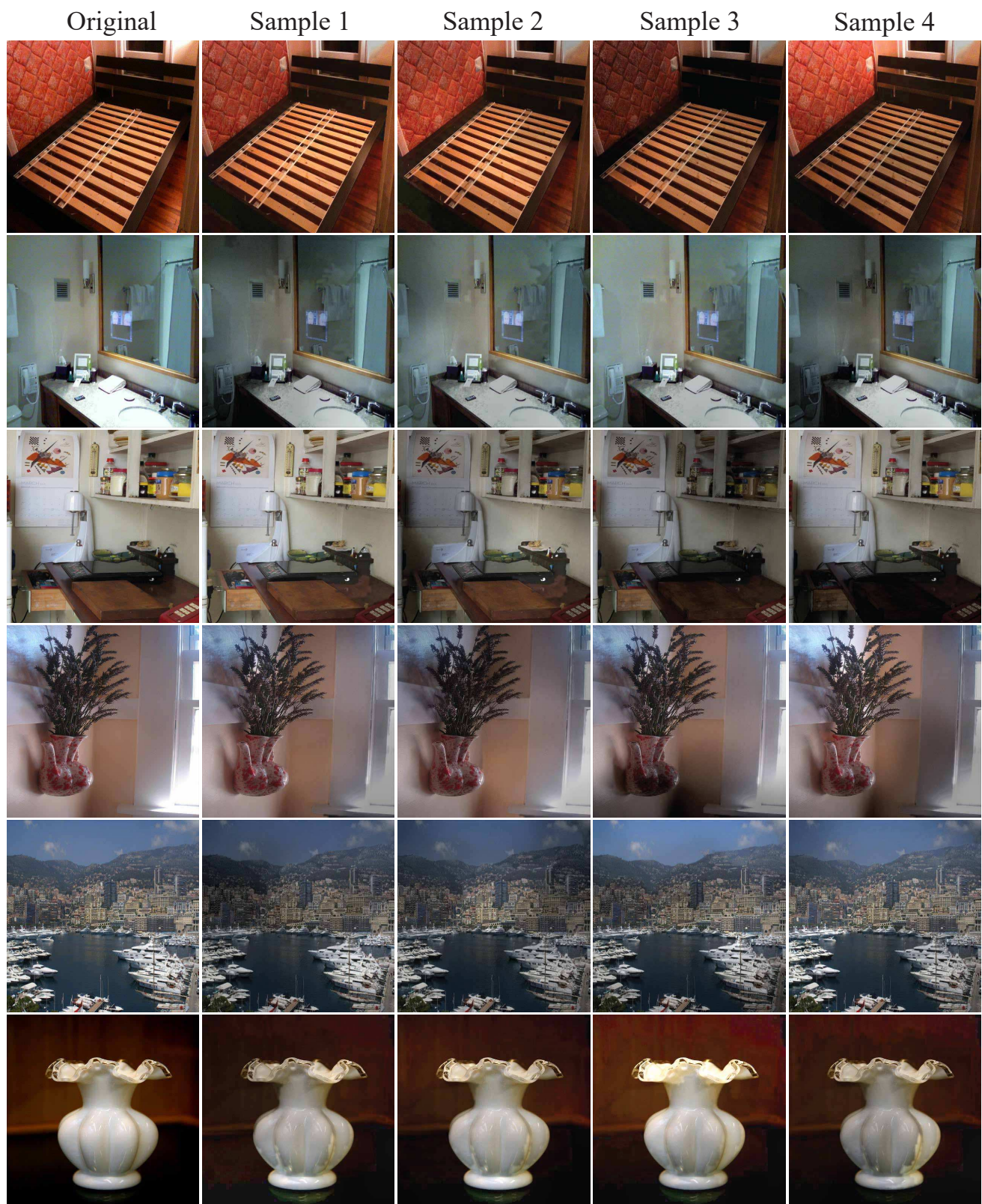


Figure 11. Photo relighting results part 3.



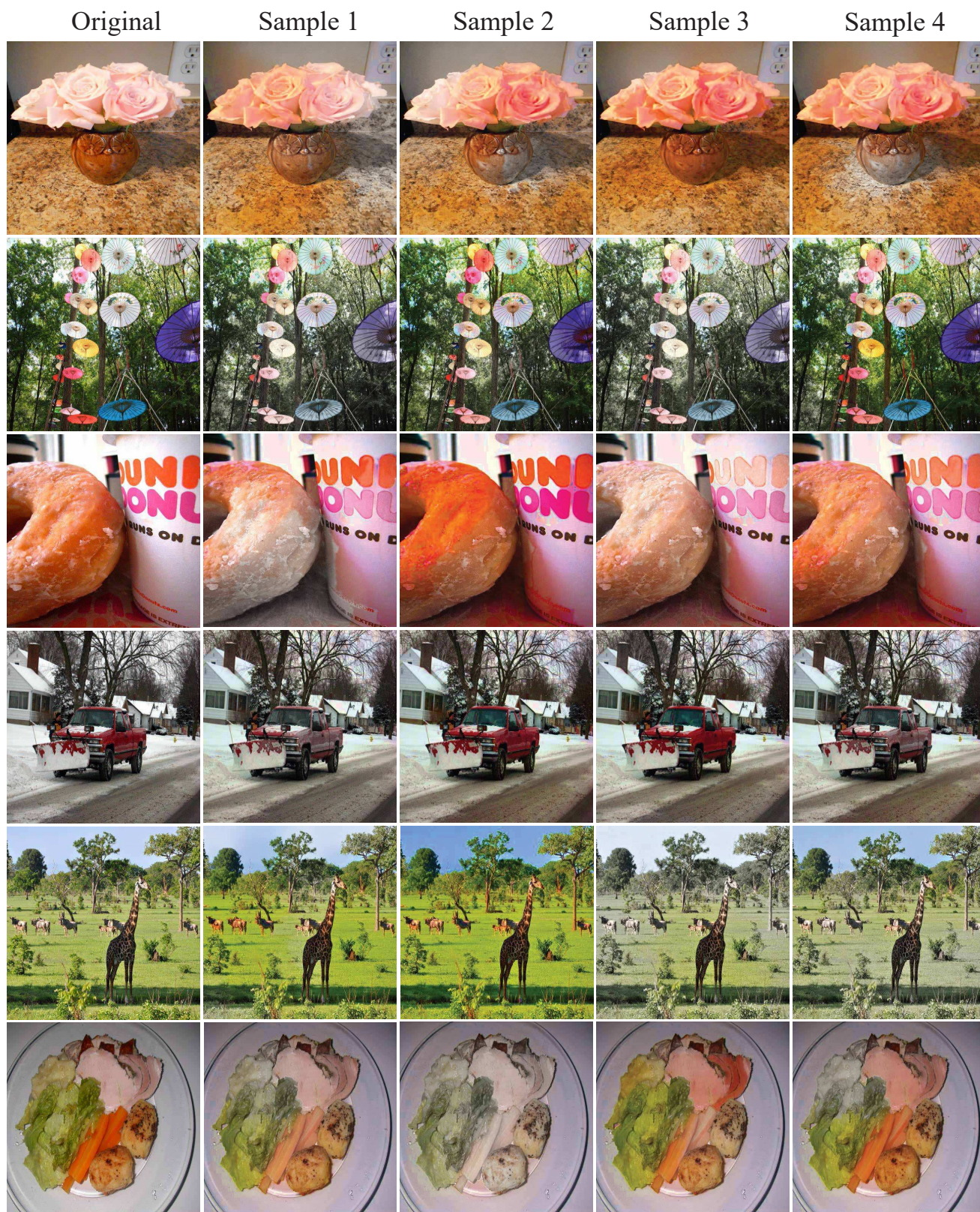


Figure 12. Image resaturation results part 1.





Figure 13. Image resaturation results part 2.



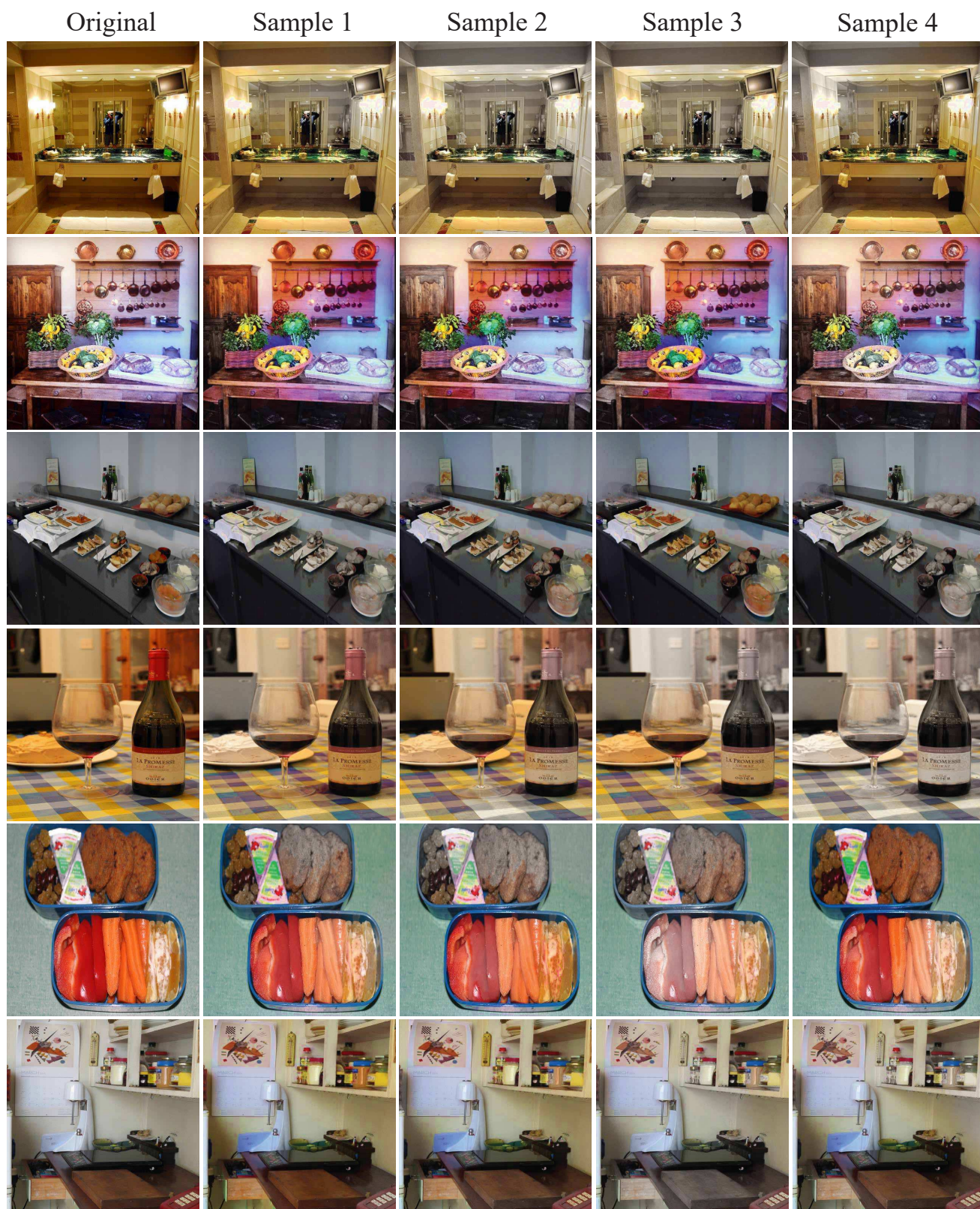


Figure 14. Image resaturation results part 3.

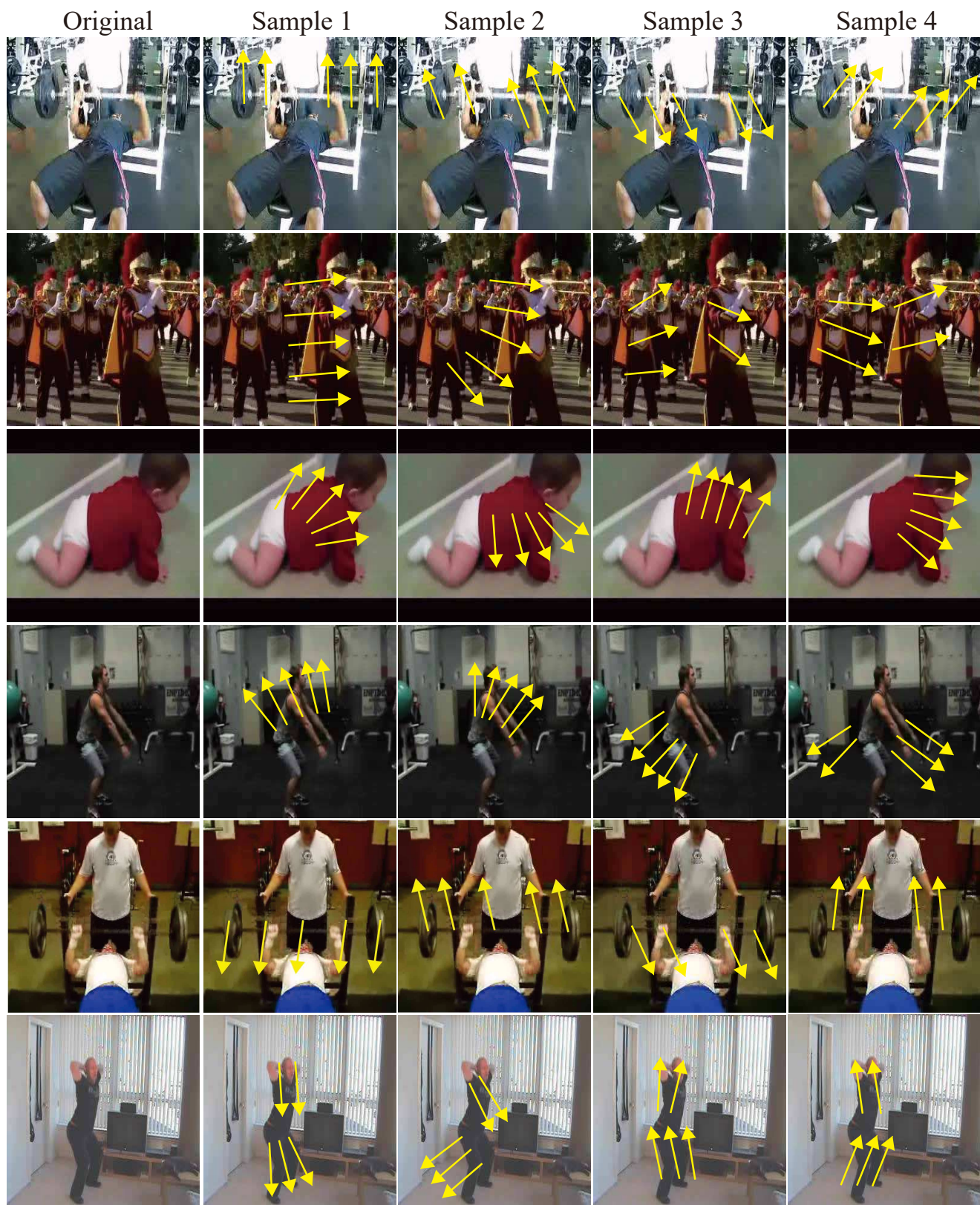


Figure 15. Motion prediction results part 1.



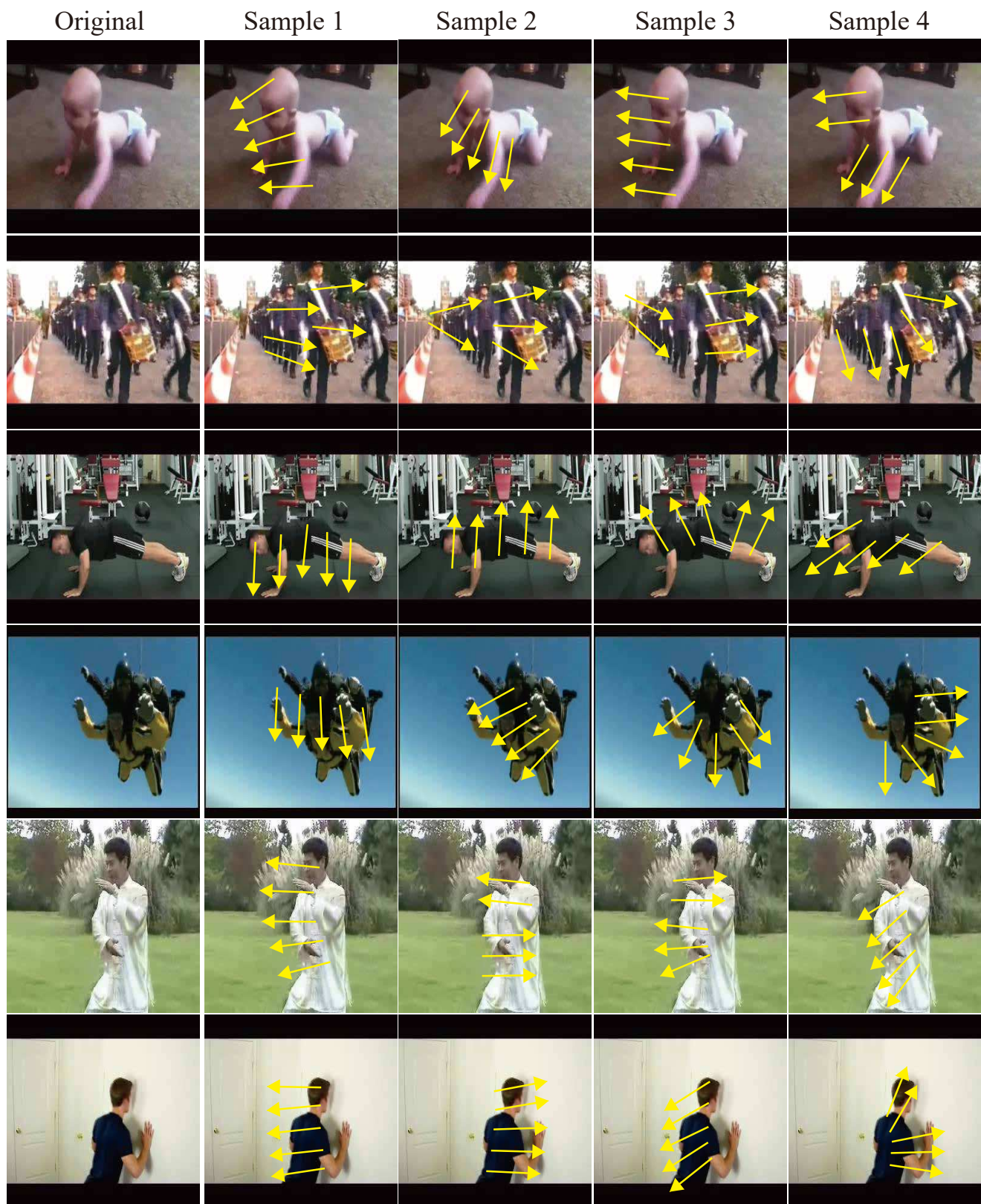


Figure 16. Motion prediction results part 2.